Article

β-Defensin 19/119 mediates sperm chemotaxis and is associated with idiopathic infertility

Graphical abstract
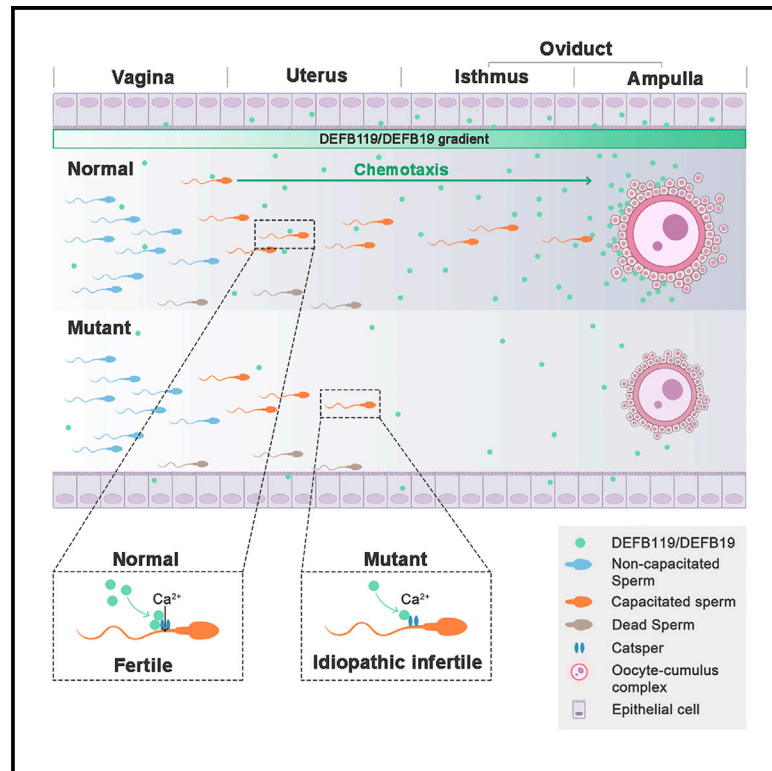
Authors

Xiaofeng Li, Chun Yuan, Jianwu Shi, ..., Jiaying Liu, Hao Chen, Kin Lam Fok

Correspondence

zengxuhui@ntu.edu.cn (X.Z.),
jyliu_nj@126.com (J.L.),
chenhao@ntu.edu.cn (H.C.),
ellisfok@cuhk.edu.hk (K.L.F.)

In brief

Li et al. describe the multistage chemotaxis in the female reproductive tract that guides the sperm to the fertilization site and the oocyte by the physiological chemoattractant DEFB19/119. Mutations in DEFB119 gene may underlie unexplained infertility in women.

Highlights

- DEFB119/DEFB19 are physiological chemoattractants for sperm chemotaxis in human and mouse

- DEFB19 mediates multistage chemotaxis along the female reproductive tract

- DEFB119 gene mutations are associated with idiopathic infertility in women

CellPress

Cell Reports Medicine

Article

β-Defensin 19/119 mediates sperm chemotaxis and is associated with idiopathic infertility

Xiaofeng Li,[1,2,11] Chun Yuan,[3,11] Jianwu Shi,[4,11] Hang Kang,[4] Yufei Chen,[4] Yonggang Duan,[5] Jing Jin,[2] Lai Ping Cheung,[6] Tin Chiu Li,[6] Ying Liu,[3] Yugui Cui,[3] Ye Chun Ruan,[2,10] Xiaohua Jiang,[2,7] Zhiming Cai,[8] Hsiao Chang Chan,[2,7,9] Ling Ji,[1] Xuhui Zeng,[4,*] Jiaying Liu,[3,*] Hao Chen,[4,*] and Kin Lam Fok[2,7,9,12,*]

[1]Department of Laboratory Medicine, Peking University Shenzhen Hospital, Lianhua Road No. 1120, Futian District, Shenzhen, PR China
[2]Epithelial Cell Biology Research Center, School of Biomedical Sciences, Faculty of Medicine, The Chinese University of Hong Kong, Hong Kong SAR, PR China
[3]State Key Laboratory of Reproductive Medicine, Clinical Center of Reproductive Medicine, First Affiliated Hospital, Nanjing Medical University, Nanjing, PR China
[4]Institute of Reproductive Medicine, Medical School of Nantong University, Nantong, PR China
[5]The University of Hong Kong-Shenzhen Hospital, Shenzhen, PR China
[6]Department of Obstetrics and Gynaecology, Faculty of Medicine, The Chinese University of Hong Kong, Hong Kong SAR, PR China
[7]School of Biomedical Sciences Core Laboratory, Shenzhen Research Institute, The Chinese University of Hong Kong, Shenzhen, PR China
[8]Shenzhen Key Laboratory of Genitourinary Tumor, Shenzhen Second People's Hospital, First Affiliated Hospital of Shenzhen University, Shenzhen, PR China
[9]Sichuan University-The Chinese University of Hong Kong Joint Laboratory for Reproductive Medicine, West China Second University Hospital, Chengdu, PR China
[10]Present address: Department of Biomedical Engineering, The Hong Kong Polytechnic University, Hong Kong SAR, PR China
[11]These authors contributed equally
[12]Lead contact
*Correspondence: zengxuhui@ntu.edu.cn (X.Z.), jyliu_nj@126.com (J.L.), chenhao@ntu.edu.cn (H.C.), ellisfok@cuhk.edu.hk (K.L.F.)
https://doi.org/10.1016/j.xcrm.2022.100825

SUMMARY

Sperm chemotaxis is required for guiding sperm toward the egg. However, the molecular identity of physiological chemoattractant and its involvement in infertility remain elusive. Here, we identify DEFB19/119 (mouse/human orthologs) as a physiological sperm chemoattractant. The epithelia of the female reproductive tract and the cumulus-oocyte complex secrete DEFB19/119 that elicits calcium mobilization via the CatSper channel and induces sperm chemotaxis in capacitated sperm. Manipulating the level of DEFB19 in mice determines the number of sperm arriving at the fertilization site. Importantly, we identify exon mutations in the *DEFB119* gene in idiopathic infertile women with low level of DEFB119 in the follicular fluid. The level of DEFB119 correlates with the chemotactic potency of follicular fluid and predicts the infertile outcome with positive correlation. This study reveals the pivotal role of DEFB19/119 in sperm chemotaxis and demonstrates its potential application in the diagnosis of idiopathic infertility.

INTRODUCTION

Infertility affects over 15% of couples worldwide. Despite the advancement in the diagnosis and treatment of infertility, the underlying cause of around 20% of these infertile cases remains unexplained.[1] The migration of sperm in the female reproductive tract (FRT) plays an essential role in fertilization and is influenced by the fluid movement, thermal gradient, and chemical gradient.[2–8] The chemical guidance of human sperm, also known as sperm chemotaxis, has long been observed in mammals and is considered an important mechanism in guiding sperm toward the egg.[9] Under physiological condition, sperm chemotaxis occurs in the FRT with the follicular fluid (FF), the cumulus-oocyte complex (COC), and oviductal fluid as possible physiological sources of chemoattractant.[10] Hitherto, the contribution of FRT chemoattractant to infertility remains elusive.

One of the most well-established sources of chemoattractant is FF. Intriguingly, the release of FF is a single event at ovulation, and therefore, it is unlikely to sustain the supply of chemoattractant(s) throughout the survival period of the egg. Since conditioned media from the matured egg and surrounding cumulus cells have been observed to be chemotactically active,[11] and an oocyte-derived chemoattractant has been characterized,[12] the COC is considered another important source of chemoattractant to sustain sperm chemotaxis after ovulation. It is postulated that sperm can undergo multistep chemotaxis in response to different chemoattractants to complete the long voyage in the FRT.[9] These chemoattractants may elicit different behavioral responses in sperm that enable them to travel a much longer distance compared with a single chemoattractant gradient.[9] Progesterone is one of the most studied chemoattractants found in FF and COC, which has been shown to elicit calcium
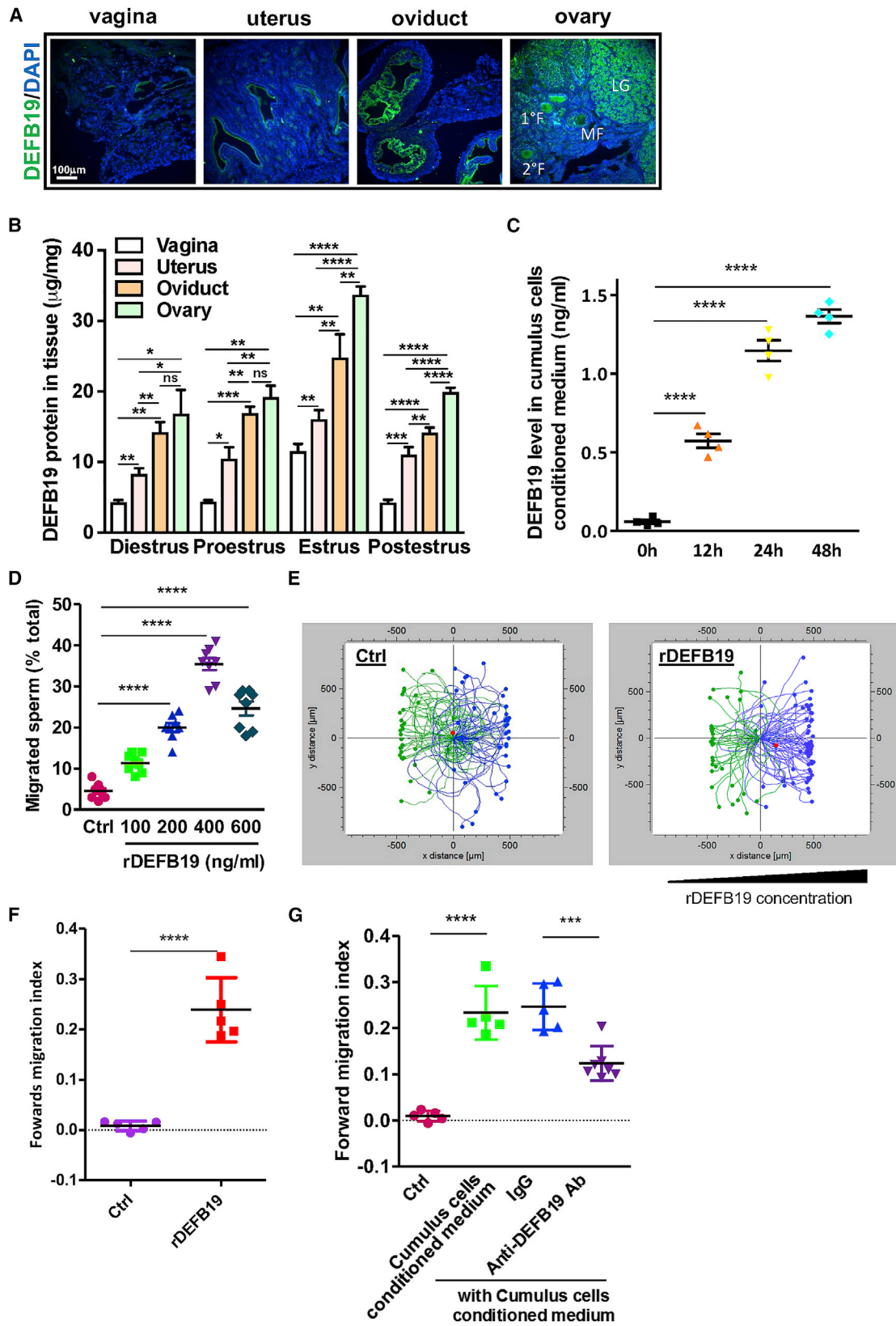
(legend on next page)

mobilization involved in chemotaxis.[13–15] However, the chemotactic potential of progesterone has only been demonstrated by *in vitro* studies.[9,10] Under these conditions, substances of unknown physiological sources can also be chemotactically active.[16] Nonetheless, the involvement of any of these potential chemoattractants in sperm chemotaxis has not been demonstrated *in vivo*.

Beta-defensin family is a group of small antimicrobial peptides mainly expressed and secreted by the epithelial linings of various organ systems, including the reproductive tract.[17] In host defense, β-defensins are also chemotactically active to immune cells. Besides, β-defensins are also expressed in the reproductive tract and reported to be involved in sperm motility affecting their fertilizing capacity.[18–21] Given the chemotactic ability of β-defensins and their capability of promoting sperm motility, we investigated the possible involvement of β-defensins in sperm chemotaxis and infertility. Here, we show that human DEFB119 and its mouse ortholog DEFB19 are chemotactically active in sperm chemotaxis assays *in vitro*. Manipulating the level of DEFB19 in mouse oviduct alters the number of sperm at the fertilization site and the fertility outcome *in vivo*. More importantly, we revealed that DEFB119 level was associated with the chemotactic potency of FF in idiopathic infertile women who carried exon mutations of *DEFB119*. Further, we have demonstrated the potential of DEFB119 in the diagnosis of idiopathic infertility.

RESULTS

DEFB19 is secreted by COC and expressed along the FRT

First, we sought to investigate the expression profile of β-defensins in FRT to identify potential chemoattractants. We selected six candidate β-defensins (*Defb8*, *15*, *19*, *35*, *42,* and *45*) shown to be expressed by cumulus cells and oocytes in the mouse from the Gene Expression Omnibus database and a ubiquitously expressed β-defensin *Defb1*, which the human homolog has been shown to be involved in sperm motility.[21] In the gene expression experiment, we found that six of the seven candidate β-defensins were expressed in the ovaries of mature mice (Figure S1). The expression of *Defb1* was highest in the vagina and gradually decreased in the uterus/oviduct and reached a low level in the ovary. We focused on *Defb19* because of its ascending gradient expression from the vagina toward the oviduct with robust expression in the ovary (Figure 1A). The expression of *Defb19* and the level of DEFB19 protein were estrus cycle dependent and peaked at the estrus phase when ovulation occurs (Figures 1B and S2A).[22] In the oviduct, the expression of DEFB19 was higher in the ampulla compared with the isthmus (Figures S2B and S2C). Using a primary culture of mouse cumulus cells, we observed the mRNA expression in the cumulus cells and the secretion of DEFB19 protein to the cumulus cell-conditioned media (Figures 1C and S2D).

DEFB19 elicits mouse sperm chemotaxis *in vitro*

We first assessed the chemotactic activity of DEFB19 by ascending accumulation gradient assay (AAGA).[9] We synthesized DEFB19 and analyzed its intramolecular disulfide bonds, which are indispensable for the activity of the defensin family.[23,24] The recombinant DEFB19 (rDEFB19) possessed proper disulfide bonds by LC-MS/MS as observed in the β-defensin family members (Figure S3).[25] Then, we established ascending gradients of rDEFB19 (100–600 ng/mL) from the upper chamber toward the lower chamber. We confirmed the establishment of DEFB19 gradient using a fluorescent-conjugated rDEFB19 (Figure S4A). Capacitated mouse sperm were seeded in the lower chambers, and the accumulation of sperm that migrated across the chambers was measured. DEFB19 dose dependently increased the percentage of sperm that migrated toward the upper chamber, with the highest migration rate observed at 400 ng/mL (Figure 1D). The same dose of rDEFB19 also attracted a markedly higher percentage of sperm in choice assay compared with vehicle control (Figures S4B and S4C).

Further, we performed a directionality-based assay using the Zigmond-like chamber (μ-slide chemotaxis[3D]), which has been used to quantify sperm chemotaxis.[26–28] In this system, the movement of sperm toward the chemoattractant was visualized, and the direction and distance of sperm movement were quantified. Similarly, the DEFB19 gradient was confirmed by a fluorescent-conjugated rDEFB19 (Figure S4D). Consistent with AAGA and choice assay, rDEFB19 was chemotactically active to mouse sperm as indicated by the increase in the forward migration index of directionality assay (Figures 1E and 1F). In corroboration with the previous observations on the lack of

Figure 1. DEFB19 is expressed in mouse female reproductive tract and induces chemotaxis in mouse sperm

(A) Representative immunofluorescence images showing the expression of DEFB19 (green) in mouse vagina, uterus, oviduct, and ovary (n = 3 mice). Nuclei were counterstained by DAPI (blue). Scale bar represents 100 μm.

(B and C) ELISA results showing the protein level of DEFB19 in different parts of the female reproductive tract at indicated phases of the estrous cycle (B, n = 5 mice) and in conditioned medium collected at indicated time points after culturing with primary mouse cumulus cells (C, n = 4 experiments, three mice were used in each experiment). Data are presented as means ± SD. *p < 0.05; **p < 0.01; ***p < 0.001; ****p < 0.0001.

(D) Ascending accumulation gradient assay showing the percentage of sperm accumulated in the upper chamber in the presence of an indicated amount of recombinant DEFB19 (rDEFB19) or vehicle control (Ctrl) (n = 8 experiments).

(E) Representative motion track of directionality-based assay showing the swimming direction of sperm in response to rDEFB19 (400 ng/mL) or vehicle control (Ctrl). All the long trajectories in the gradient direction (purple tracks) and in the opposite direction (green tracks) were used for analysis. Red dots indicate the average migration distance of the selected sperm.

(F) Quantification of the forward migration index is shown (F, n = 5 experiments), and the concentration of rDEFB19 was 400 ng/mL.

(G) Forward migration index showing the swimming direction of sperm in response to conditioned medium of primary mouse cumulus cells or control medium (n = 5 experiments) and cumulus cell-conditioned medium with anti-DEFB19 neutralizing antibody (n = 7 experiments, 20 μg/mL) or normal IgG (n = 5 experiments, 20 μg/mL). Data are presented as means ± SD, compared by Student's t test (F) or one-way ANOVA with Tukey's post hoc test (D and G). ***p < 0.001; ****p < 0.0001.
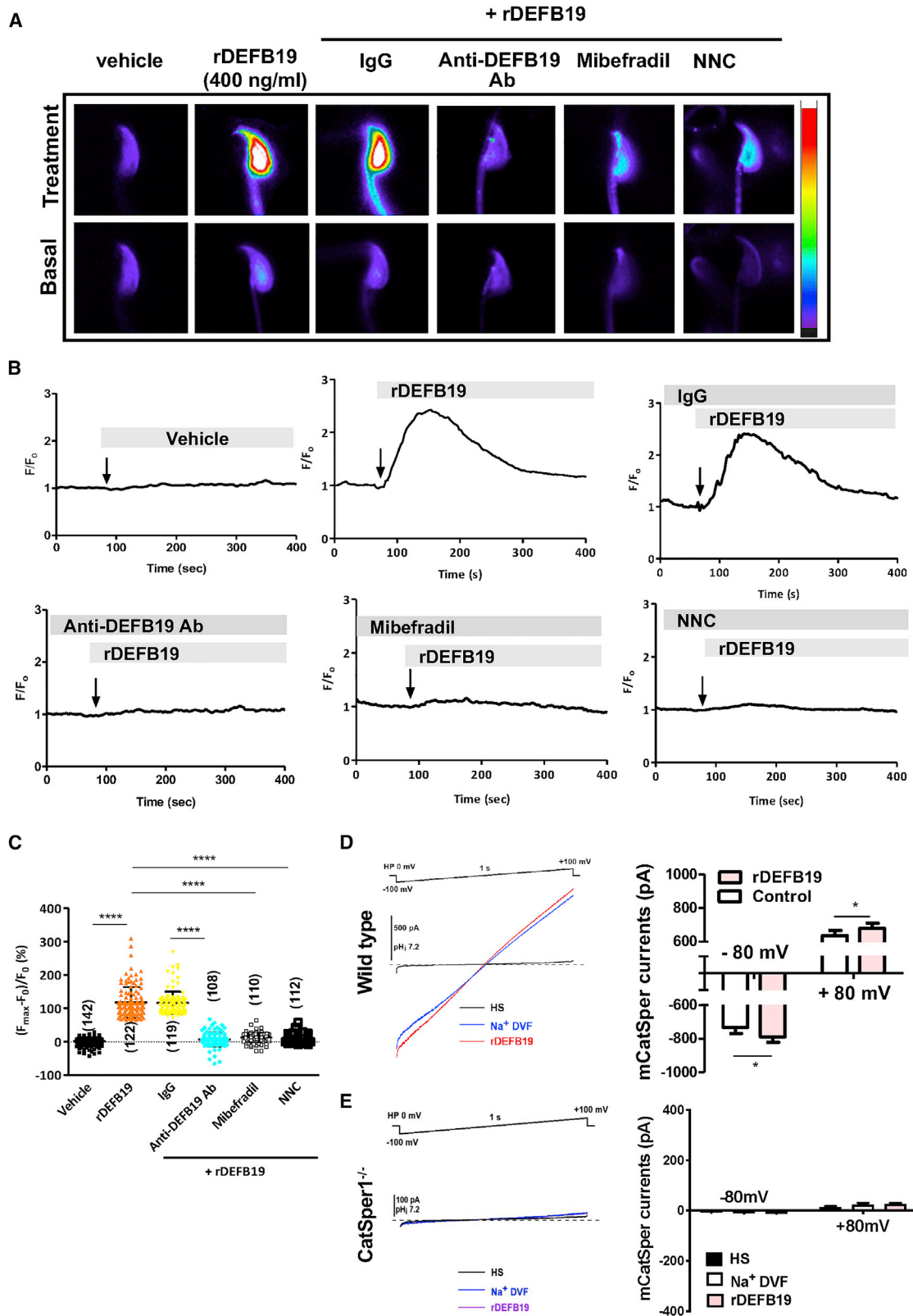
(legend on next page)

chemotactic responsiveness in non-capacitated sperm, DEFB19-induced sperm chemotaxis was markedly higher in capacitated sperm, whereas that in non-capacitated sperm was negligible (Figure S4E). Similar chemotactic effect was not observed in sperm treated with mouse DEFB1 (Figures S4F and S4G), supporting the specificity of DEFB19 chemotactic activity toward mouse sperm.

We next sought to examine the contribution of DEFB19 to the chemotactic activity of FF. To mimic mouse FF, we collected the conditioned medium from a primary culture of mouse cumulus cells and examined its chemotactic activity. We depleted functional DEFB19 in the conditioned medium by a neutralizing antibody against DEFB19. The result from directionality-based assay revealed that the chemotactic activities of conditioned medium were significantly suppressed by immunodepletion of DEFB19 (Figure 1G), suggesting the physiological relevance of DEFB19 in mouse sperm chemotaxis.

DEFB19 triggers CatSper-dependent Ca^{2+} mobilization

We further examined whether DEFB19 could trigger calcium mobilization since it plays central roles in sperm functions such as motility and chemotaxis during the voyage in the FRT.[29] In human sperm, the principal Ca^{2+} channel CatSper triggers Ca^{2+} influx associated with motility and chemotaxis.[30–33] Thus, we also examined the possible involvement of CatSper channel in DEFB19-induced Ca^{2+} response. We found that DEFB19 was co-localized and interacted with the CatSper1 channel in the principal piece of sperm (Figure S5). By measuring the intracellular Ca^{2+} in the head region,[34,35] we revealed that rDEFB19 markedly elevated intracellular Ca^{2+} level in mouse sperm (Figures 2A–2C). The DEFB19-induced Ca^{2+} mobilization could be abolished by corresponding neutralizing antibodies against DEFB19. The Ca^{2+} responses were also significantly inhibited by CatSper channel inhibitors mibefradil or NNC-55-0396 (NNC) (Figures 2A–2C), suggesting the involvement of CatSper channel in the DEFB19-induced Ca^{2+} elevation. Indeed, sperm patch-clamp experiment revealed that rDEFB19 induces CatSper channel activity (Figure 2D). Similar induction was not observed in sperm obtained from $CatSper1^{-/-}$ mouse lacking the CatSper channel activity (Figures 2E and S6).

Sperm hyperactivation, which is also mediated by CatSper channel,[36,37] has been proposed to be involved in sperm chemotaxis.[27,38] Therefore, we examined the hyperactivated motility and kinetic parameters of capacitated sperm in response to rDEFB19 treatment by computer-assisted sperm analysis (CASA). We observed a significant increase in curvilinear velocity (VCL), average path velocity (VAP), and straight-line velocity (VSL)

(Figures S7A–S7C). In line with the increase in motion parameters, rDEFB19 treatment markedly increased the percentage of sperm with hyperactivated motility to 26% ± 4.4% compared with that in the vehicle control (15.88% ± 3.3%) (Figure S7D). The rDEFB19-induced hyperactivation was blunted by the DEFB19 neutralizing antibody or mibefradil (Figure S7D), suggesting that DEFB19 induces hyperactivation through CatSper channel.

DEFB19 elicits mouse sperm chemotaxis *in vivo*

Next, we assessed the involvement of DEFB19 in mouse sperm chemotaxis *in vivo*. DEFB19 was robustly expressed in developing follicles that later form the COC (Figure 1). To test the contribution of DEFB19 from COC, we surgically ligated the ovary-oviduct connection in mice 6–8 h after mating with males as described previously.[39–41] As a result, the COC was absent in ligated oviduct. In this ligation model, the number of sperm that arrived at the ligated oviducts was significantly lower than that in contralateral sham-operated non-ligated oviducts (Figures S8A–S8C), suggesting a reduction of chemotactic activity in FRT due to the absence of COC. Next, we overexpressed *Defb19* in the ligated oviduct to restore the level of DEFB19 (Figures S8D and S8E). Overexpression of DEFB19 significantly restored the number of sperm that arrived at the ligated oviduct compared with the contralateral ligated oviduct transfected with vector control (Figures S8F and S8H).

To confirm the involvement of DEFB19 *in vivo*, we knocked down DEFB19 by injecting two individual designs of siRNAs against DEFB19 (siDEFB19#1 or siDEFB19#2) or control siRNAs (siNC) into the oviducts (Figure 3A). As expected, the number of sperm detected in the siDEFB19-injected oviducts was significantly lower than that in contralateral control siRNA-injected oviducts (Figures 3B and 3C). Furthermore, we examined the fertility outcome after knocking down DEFB19 by housing the siRNAs-injected female mice with male mice. Consistent with the decreased number of sperm, the number of implanted embryos in DEFB19 knocked-down oviducts was significantly lower than that in the contralateral control oviducts (Figures 3D–3G). These results confirm the involvement of DEFB19 in sperm chemotaxis and its essential role in fertility.

Knockout of Defb19 impairs chemotaxis and fertility potency in mice

Previous studies indicated *Defb19* is primarily expressed in the mouse reproductive system.[42] To better understand the involvement of DEFB19 in mouse sperm chemotaxis *in vivo*, we established *Defb19*-knockout (KO) mice using the CRISPR-Cas9 technology by deleting exon 1 and exon 2 of *Defb19* gene (Figure 4A).

Figure 2. DEFB19 triggers CatSper-dependent Ca^{2+} mobilization

(A and B) Representative fluorescence images (A) and time course tracing (B) of mouse sperm loaded with Fluo-4, a Ca^{2+} sensitive dye, before (basal) and after the addition of rDEFB19 (400 ng/mL) with or without pretreatment of normal IgG (20 μg/mL), anti-DEFB19 antibody (20 μg/mL), Catsper inhibitor mibefradil (40 μM), and NNC (NNC 55–0396, 2 μM).

(C) Quantification of percentage change in intracellular Ca^{2+} level (($F_{max} - F_0$)/F_0(%)) (numbers in parenthesis represent the number of sperm recorded in four independent experiments).

(D and E) Representative patch-clamp recording of whole-cell currents in wild-type mouse sperm (D) or $CatSper1^{-/-}$ mouse sperm (E) elicited by 1-s voltage ramp from −100 to +100 mV with pipette pH (pHi) at 7.2. From the same patch, the monovalent CatSper currents in wild-type sperm were recorded after application with DVF or DVF added with test factors (rDEFB19, 400 ng/mL) (D, left panel) (n = 6 sperm). With *CatSper1* deleted, the subtle and similar currents detected in both high saline solution (HS) and DVF solutions confirmed the deficiency of CatSper currents (E, left panel). Corresponding statistical analysis are shown on the right panel (n = 5 sperm). Data are presented as means ± SD. *p < 0.05; ****p < 0.0001.
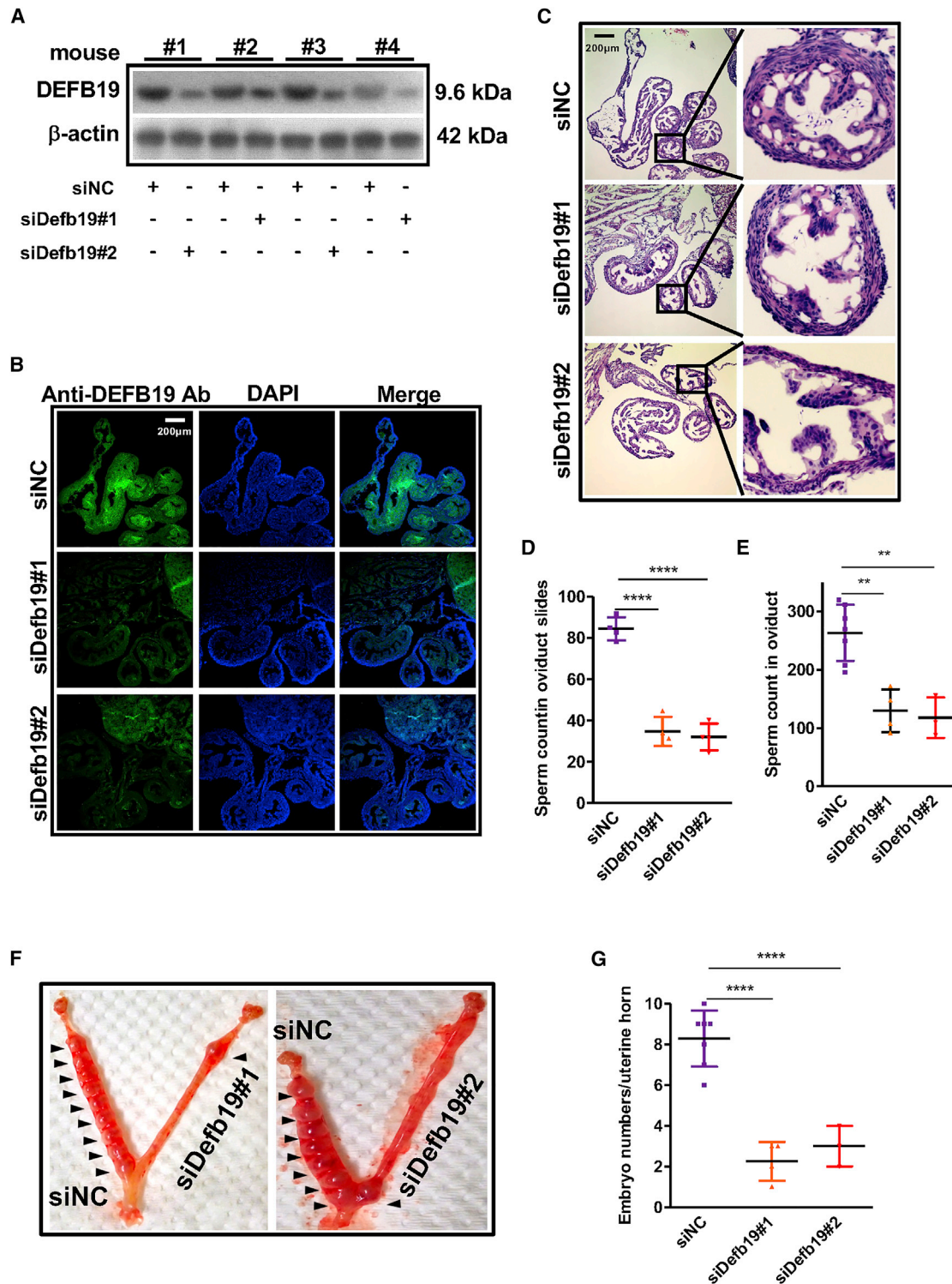
Figure 3. Knockdown of *Defb19* in oviduct perturbs sperm chemotaxis *in vivo*

(A and B) Western blot results (A) and representative immunofluorescence staining (B) showing the expression of DEFB19 in the oviduct of matured female mice upon *in vivo* transfection of two individual designs of siRNA targeting DEFB19 (siDefb19#1 and siDefb19#2, 50 pmol) or control siRNA (siNC, 50 pmol) (n = 4 experiments).

(C) Representative H&E staining showing the sperm that arrived at the oviduct of matured female mice with or without knockdown of DEFB19 (n = 4 experiments). Scale bar represents 200 μm.

(legend continued on next page)

We performed PCR and immunofluorescence staining to confirm the absence of DEFB19 in the KO mice (Figures 4B and S9A). *Defb19*-KO female mice show complete follicle development with normal histology of the FRT and normal body weight (Figures S9B and S9C). However, female mice were subfertile and sired a lower number of litters compared with the wild type (Figure 4C). To investigate if the subfertility stemmed from the defects in sperm chemotaxis in the KO mice, we inseminated the sperm obtained from wild-type (WT) male mice to the uterus of WT or KO female mice. The result showed that the number of sperm detected in the oviducts of KO mice was significantly lower than that in the oviducts of WT mice (Figures 4D–4F). Consistent with the decreased number of sperm, the average number of implanted embryos in *Defb19*-KO oviducts was significantly lowered than that in the WT oviducts (Figures S9D and S9E). Next, we collected the conditioned medium from a primary culture of WT and KO mouse cumulus cells and examined its chemotactic activity. The result revealed that the chemotactic activity of conditioned medium from KO mice was significantly weaker than that of WT mice (Figures 4G–4I). These results indicate the vital role of *Defb19* in sperm chemotaxis and fertility *in vivo*.

DEFB119 elicits human sperm chemotaxis

We next examined if the DEFB19-mediated sperm chemotaxis is conserved in humans. *Defb19* is the mouse ortholog of human *DEFB119*. Similar to mouse *Defb19*, we found that human *DEFB119* was expressed in human cumulus cells (Figure S10). To examine the chemotactic activity of DEFB119 toward human sperm, we tested various doses of GST-tagged DEFB119 (GST-DEFB119, 100–1200 ng/mL), which also possessed disulfide bonds commonly observed in β-defensin members (Figure S11), using AAGA. Consistent with the result in mouse sperm, GST-DEFB119 formed a gradient (Figure S12A), and it attracted human sperm in a dose-dependent manner (Figure 5A). The same dose of GST-DEFB119 also attracted a higher percentage of capacitated sperm in the choice assay and directionality assay (Figures 5B and S12B–S12E), and it markedly increased the percentage of sperm with hyperactivated motility compared with those treated with the GST tag alone (Figure S13). Notably, an effective dose of recombinant DEFB1, a ubiquitously expressed β-defensin known to maintain sperm motility,[21] induced a modest increase in forward migration index in directionality assay but no significant chemotactic activity toward human sperm in directionality assay, AAGA, and choice assay (Figures 5A, 5B, and S12B), suggesting that the chemotactic activity was specific to DEFB119.

Lastly, we tested the effect of DEFB119 on Ca^{2+} mobilization. Consistent with the results in mouse sperm, GST-DEFB119 markedly elevated the intracellular Ca^{2+} level in human sperm,

which could be blunted by neutralizing antibodies against DEFB119 (Figures 5C–5G). The Ca^{2+} responses induced by DEFB119 were considerably higher than that caused by DEFB1. The GST-DEFB119-induced Ca^{2+} responses were also significantly inhibited by mibefradil or NNC 55–0396 (Figure 5G). Consistent with the Ca^{2+} response, DEFB119 induced CatSper channel activity that can be blunted by another CatSper inhibitor RU1968F1[43](Figures 5H and 5I) and anti-DEFB119 antibodies (Figure S14). GST-DEFB119 taken up by the sperm was in close proximity to CatSper1 (Figure S15). These results suggest a conserved mechanism underlying the effect of DEFB19/119 on sperm chemotaxis.

Deficiency of DEFB119 is associated with unexplained infertility

Hitherto, few reports have linked sperm chemotaxis with infertility. Two preliminary studies suggested that a decreased sensitivity of sperm to artificial chemoattractant bourgeonal may be associated with idiopathic infertility.[44,45] However, the physiological source of odorant or other related molecules remains controversial. Moreover, the involvement of FRT-induced sperm chemotaxis in idiopathic infertility has not been investigated. To examine the potential involvement of DEFB119-mediated sperm chemotaxis in infertile cases, we compared the FF from 120 idiopathic infertile women and 120 control subjects (partner of male factor infertility) for the expression level of DEFB119 and the ability of FF samples to induce sperm chemotaxis. The clinical information of these patients is shown in Table S1. The results indicated that the level of DEFB119 protein as well as the chemotactic activity were significantly lowered in FF obtained from idiopathic infertile women (Figures 6A and 6B).

Moreover, DEFB119 protein level was positively correlated with chemotaxis potency (Figure 6C). We screened for polymorphisms and mutations in the *DEFB119* gene from the blood samples collected from 104 control and 105 idiopathic infertile women of the same cohort. Six single mutations in the coding region were identified in six patients but not in the control subjects (Figure 6D and Table S2). Among these, the homozygous nonsense C55X mutation (patient number 11) and the heterozygous missense C56S mutation (patient number 27) were predicted to be deleterious by three complementary nsSNV scoring algorithms (Table S2), including SIFT,[46] PolyPhen2,[47] and M-CAP.[48,49] The K40E mutation (patient number 69) and the E69G mutation (patient number N108) were predicted to be deleterious by two complementary nsSNV scoring algorithms (Table S2). Indeed, the FF obtained from homozygous C55X mutation (N11) has an undetectable level of DEFB119 protein and the weakest FF chemotaxis potency (Figures 6A and 6B). We also found 19 mutations in the intron region of

(D) Quantification of sperm count in the oviduct sections of DEFB19 knockdown or control siRNA transfected oviduct of matured female mice. At least five random fields were counted for each mouse (n = 4 mice).

(E) Quantification of sperm count obtained by flushing of the DEFB19 knockdown or control siRNA transfected oviduct of matured female mice (siNC, n = 7 mice; siDefb19#1, n = 4 mice; siDefb19#2, n = 3 mice).

(F) Representative images showing the number of the implanted embryos in the uterine horn connected to the DEFB19 knockdown or control siRNA transfected oviduct.

(G) Quantification of embryo numbers in uterine horn (siNC, n = 7 mice; siDefb19#1, n = 4 mice; siDefb19#2, n = 3 mice). Data are presented as means ± SD, compared by one-way ANOVA with Tukey's post hoc test.

A

gRNA1   gRNA2

5´   3´

Defb19 Exon1   *Defb19* Exon2   *Defb21* Exon

gRNA1 (matches reverse strand of gene): GCCGAGCAGTTCACTAGATGTGG
gRNA2 (matches forward strand of gene): ATTGGGCTTTGCACGGTGAGAGG

B

Anti-DEFB19 Ab   DAPI   Merge

C

D

E

F

G

H

I
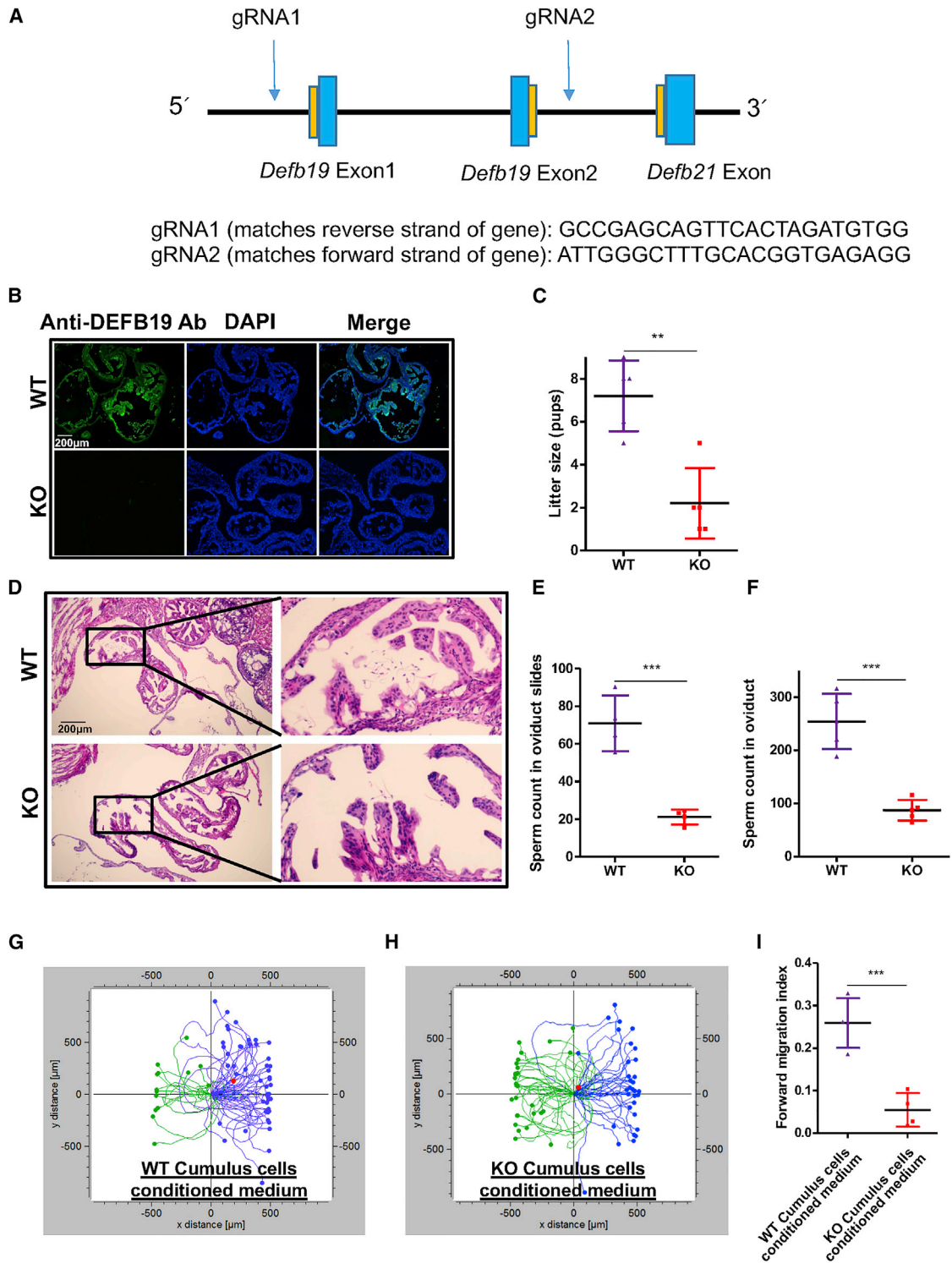
Figure 4. Knockout of Defb19 in mice perturbs sperm chemotaxis and leads to subfertility

(A) The schematic illustration of the targeting strategy for generating *Defb19*-knockout mice. A deleting mutation was generated by deleting exon 1 and exon 2 of *Defb19*. The gRNA pairs used in this mouse are shown below.

(B) Representative immunofluorescence staining showing the expression of DEFB19 in the oviduct of WT and *Defb19*-KO female mice (n = 4 experiments).

(C) Quantity of WT and *Defb19*-KO mice litter size (n = 5 mice). **p < 0.01.

(legend continued on next page)

DEFB119. Seven of them were common to control and infertile patients, while 12 were only observed in the infertile patients. Mutations in *DEFB119* were associated with idiopathic infertility (Table 1). This result suggests that *DEFB119* is highly polymorphic and its mutations may be an etiological factor of idiopathic infertility.

To explore the diagnostic value of DEFB119 level for idiopathic infertile patients, receiver operating characteristic (ROC) curve (Figure 6E) was applied to the level of DEFB119 in the FF. The area under the ROC curve was 0.9043, which was significant ($p = 2.6 \times 10^{-27}$). Further, sensitivity and specificity of the test was calculated at various values, and a cut off value of 29.27 ng/mL was calculated at which 53.33% sensitivity and 95% specificity was observed. With this threshold, patients with DEFB119 level below the threshold (DEFB119^{low}) were associated with idiopathic infertility (Table 1). Notably, exon mutations in *DEFB119* were also associated with low DEFB119 (Table 1). Together, our results showed that deficient/defective DEFB119 ensued by the lowering of chemotactic activity in FF may be a risk factor in idiopathic infertility.

DISCUSSION

The present study has identified *DEFB119* and its mouse ortholog *Defb19* as a conserved chemoattractant for sperm chemotaxis in mammals. The chemotactic effect of DEFB19/119 is mediated by calcium mobilization via the CatSper channel. Although previous studies have revealed a plethora of substances promiscuously activate the CatSper channel,[9,37] the present study utilized the oviduct ligation model as well as genetic manipulation *in vivo* and showed that DEFB19 is involved in mouse sperm chemotaxis required for normal fertility under physiological condition (Figures 3, 4, and 5), strongly suggesting that DEFB19 is a physiological chemoattractant guiding sperm through the FRT. This notion is further supported by the observed reduction in chemotactic activities and levels of DEFB119 in the FF of POR, PCOS, and idiopathic infertile patients, which could be partially restored by treatment with rDEFB119. Notably, another physiological chemoattractant progesterone, which is produced by the COC, has also been postulated to be involved in human sperm chemotaxis via activation of the CatSper channel. Interestingly, the effect of progesterone on CatSper channel is not observed in mouse sperm. These findings together with the result from our current study suggest a multistep chemotaxis in the FRT where DEFB19/119 from oviductal epithelium attracts sperm toward the fertilization site and together with other chemoattractants, e.g., progesterone from COC to attract sperm toward the egg.

In this study, we showed that DEFB19/119 co-localized or located in close proximity to CatSper 1, an essential subunit of the CatSper channel. The close proximity permits direct protein-protein interaction where DEFB19/119 serves as the ligand. However, the molecular mechanism underlying the activation of the CatSper channel by DEFB19/119 remains unresolved. It is plausible that DEFB19/119 binds directly to the CatSper channels complex or interacts with the channel via an associated protein or signaling pathway that activates the channel directly or releases the channel from endogenous inhibition. The investigation of these possibilities requires further experimentation on the ligand binding kinetics, dose-response relationship, and molecular interaction between CatSper and DEFB19/119. A similar approach has been used to identify the unconventional endocannabinoid signaling that mediates the activation of the CatSper channel by progesterone in human sperm.[50] Nonetheless, in view of the conserved effect of DEFB19/119 on the CatSper channel in both human and mouse sperm, we postulate that the effect of DEFB19/119 is mediated by a molecular mechanism independent of the progesterone-induced unconventional endocannabinoid signaling cascade.

Previous studies have shown the crucial roles of β-defensin family members on human sperm functions. Tollner et al. have demonstrated that epididymis-specific DEFB126 modulates the leptin binding ability of sperm. Mutation in this gene is associated with male subfertility.[19] Our recent study has shown that ubiquitously expressed DEFB1 is required for maintaining sperm motility. Deficient of this gene underlies the lowered sperm motility in asthenozoospermia infertile patients.[21] The present study compared the effect of DEFB119 and DEFB1 on hyperactivated motility and sperm chemotaxis. While DEFB1 treatment could induce a modest, yet significant increase in hyperactivated motility, DEFB119 elicited a robust increase in hyperactivated motility. Moreover, DEFB119 was chemotactically active, while DEFB1 does not affect sperm chemotaxis. The present results suggest that family members of β-defensins play differential roles in sperm functions. To this end, it is noteworthy that DEFB119 is highly expressed in the testis, which suggests the presence of DEFB119 in sperm of the male reproductive tract. The physiological role(s) of DEFB119 in the testis and its potential involvement in sperm functions in the male reproductive tract warrant further investigations.

Another important finding of the present study is the association of DEFB119-mediated sperm chemotaxis with idiopathic infertility. Although following the guidance of standard infertility evaluation published by the American Society for Reproductive Medicine, the couples with unexplained infertility with all test results indicating normal are still approximately 15%–30%.[51]

(D) Representative H&E staining showing the sperm that arrived at the oviduct of WT and *Defb19*-KO female mice (n = 4 experiments). Scale bar represents 200 μm.

(E) Quantification of sperm count in the oviduct sections of WT and *Defb19*-KO female mice. At least five random fields were counted for each mouse (n = 4 mice). ***p < 0.001.

(F) Quantification of sperm count obtained by flushing oviduct of WT and *Defb19*-KO female mice (WT, n = 5 mice; KO, n = 5 mice). ***p < 0.001.

(G and H) Representative motion track of directionality-based assay showing the swimming direction of sperm in response to conditioned medium of primary mouse cumulus cells obtained from WT (G) and *Defb19*-KO (H) female mice (n = 4 experiments).

(I) Quantification of the forward migration index is shown on the right panel. Data are presented as means ± SD, compared by Student's t test. ***p < 0.001.
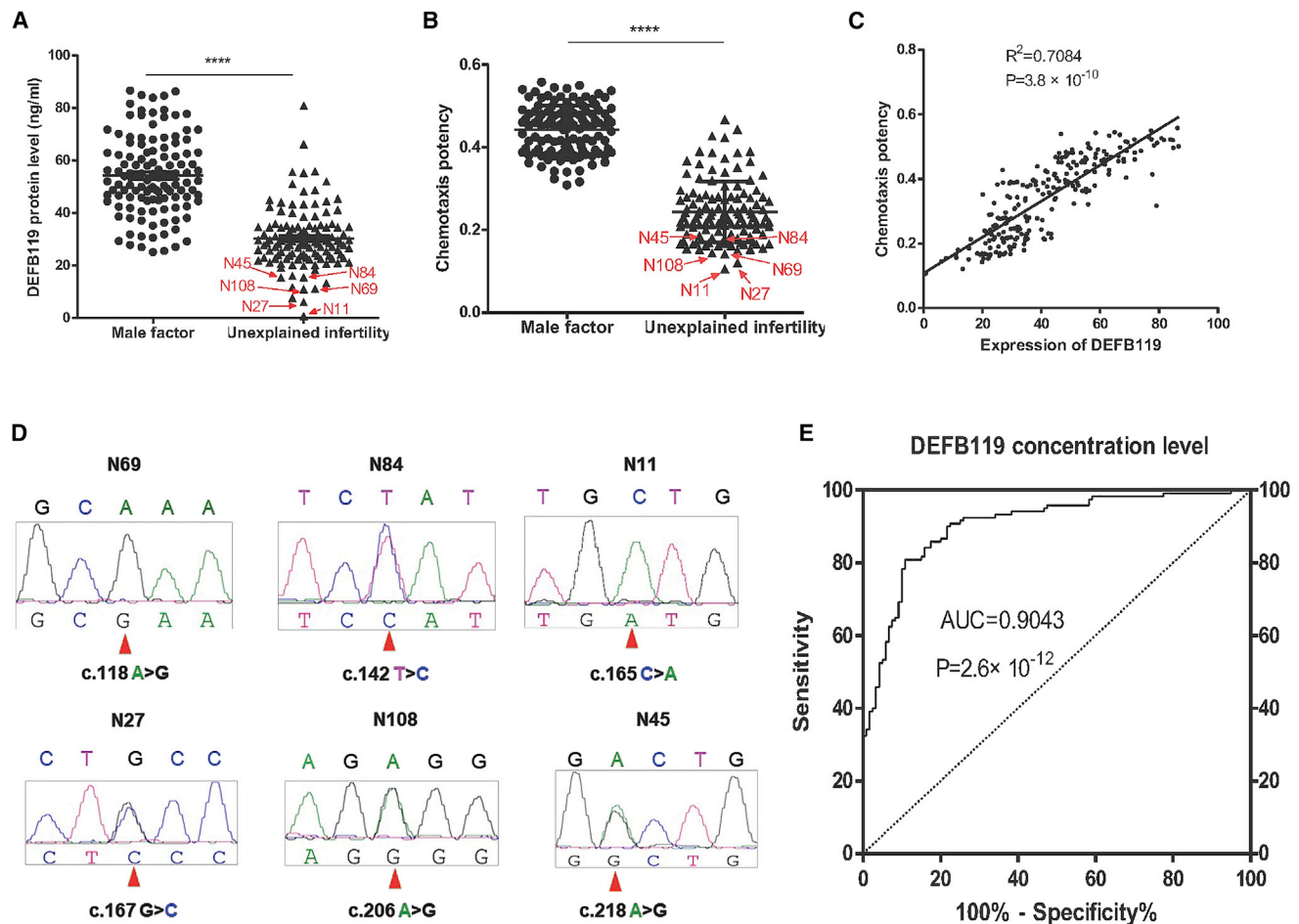
Figure 6. Mutations and protein level of DEFB119 are associated with unexplained infertility

(A and B) ELISA results (A) and directionality-based assay results (B) showing the expression of DEFB119 and chemotactic activity of the follicular fluid (FF) collected from women with idiopathic infertility (n = 120 patients). Women whose partner was diagnosed with male factor infertility were recruited as controls (n = 120 patients). The red arrows mark patient number of the CDS mutation screening. Data are presented as means ± SD, compared by Student's t test. ****p < 0.0001.

(C) Correlation analysis between DEFB119 expression and chemotaxis potency in FF obtained from idiopathic infertility patients and male factors.

(D) Sanger sequencing showing the K40E, Y48H, C55X, C56S, E69G, and D73G mutations of *DEFB119* in six idiopathic infertility patients. (E) ROC curve analysis for DEFB119 concentration levels and infertility suggesting it is a risk of idiopathic infertility.

Currently, the diagnosis of infertility is limited to sperm analysis, hormonal profiling, and structural analysis. However, a number of physiological processes that occur in the FRT, e.g., acrosome reaction and sperm chemotaxis, have not been included. Therefore, defects in these processes may have been overlooked in idiopathic infertility. Our results indicated a significant

Figure 5. Recombinant DEFB119 induces chemotaxis in human sperm

(A) Ascending accumulation gradient assay showing the percentage of sperm accumulated in the upper chamber in the presence of an indicated amount of recombinant GST-tagged DEFB119 (GST-DEFB119). GST tag or recombinant DEFB1 (800 ng/mL) was used as a control (n = 8 experiments).

(B) Quantification of the forward migration index of the directionality-based assay with sperm treated with GST-DEFB119 (800 ng/mL) in the presence or absence of anti-DEFB119 antibody (20 μg/mL) or mibefradil (40 μM) (n = 5 experiments).

(C–F) Representative fluorescence images (C) and time course tracing (D–F) of human sperm loaded with Fluo-4 before (basal) and after the addition of GFT-DEFB119 (800 ng/mL). GST tag or recombinant DEFB1 (800 ng/mL) was used as a control. (G) Quantification of percentage change in intracellular Ca^{2+} level (($F_{max} − F_0$)/F_0 (%)) with or without pretreatment of anti-DEFB119 antibody (20 μg/mL), mibefradil (40 μM), and NNC (NNC 55–0396, 2 μM) (numbers in parenthesis represent the number of sperm recorded in four independent experiments).

(H) Representative patch-clamp recording of whole-cell currents in normal human sperm elicited by 1-s voltage ramp from −100 to +100 mV with pipette pH (pH_i) at 7.2. From the same patch, the monovalent CatSper currents were recorded after application with DVF or DVF added with test factors (GST-DEFB119, 800 ng/mL or GST-DEFB119 + CatSper inhibitor RU1968F1, 10 μM).

(I) Corresponding statistical analysis of the patch-clamp recording (n = 4). Data are presented as means ± SD, compared by one-way ANOVA with Tukey's post hoc test (A, B), one-way ANOVA with Scheffe's test (G), or two-way ANOVA with multiple comparisons (I). ***p < 0.001. ****p < 0.0001.

Table 1. Association of DEFB119 gene mutations with DEFB119 protein level in follicular fluid and idiopathic infertility in women

Variable	n	Male factor freq (%)	Idiopathic infertility freq (%)	χ^2 statistics (df)	p value
Total mutation status					
Wild type	90	56 (62.2)	34 (37.8)	9.819 (1)	0.002
Total mutations	119	48 (40.3)	71 (59.7)		
Exon mutation status					
Wild type	203	104 (51.2)	99 (48.8)	N/A	0.029[a]
Exon mutations	6	0 (0)	6 (100)		
29.27 ng/mL threshold					
<29.27 ng/mL	70	6 (8.6)	64 (91.4)	67.845 (1)	0
>29.27 ng/mL	170	114 (67.1)	56 (32.9)		

29.27 ng/mL threshold difference in male factor and idiopathic infertility group.
[a]Compared by Fisher's exact test, N/A: not available.

decrease in chemotactic activity and protein level of DEFB119 in FF of idiopathic infertile women, suggesting that the deficient level or mutation of DEFB119 is an etiological factor of idiopathic infertility. Intriguingly, while the expression of DEFB19 was estrus cycle-dependent and likely under a hormone regulation in mice, the lowered level of DEFB119 was independent of abnormal hormonal profile as the idiopathic infertile cohort had a normal hormone profile and ovulation pattern. Instead, mutations in *DEFB119* gene underlie the deficient/defective function of DEFB119-mediated sperm chemotaxis in idiopathic infertility.

The potential applications of DEFB119-mediated chemotaxis are two-folded. The available assisted reproductive technologies (ARTs) for idiopathic patients are often intrauterine insemination (IUI) and *in vitro* fertilization (IVF). The lowered sperm chemotaxis activity in FF of idiopathic infertile women suggests a lower success rate of IUI as the inseminated sperm are less likely to arrive at the fertilization site. In this regard, the mutations of DEFB119 may be an indicator to predict the outcome of IUI and therefore guide the ART regimen on IUI vs. IVF. On the other hand, DEFB119 can be used for sperm selection in ART. The journey of sperm in the FRT that involved sperm functions such as capacitation and the subsequent guidance mechanisms toward the oocyte, e.g., chemotaxis and thermotaxis, is considered a natural selection process that chooses the best sperm to fertilize an oocyte. In fact, only a fraction of sperm are able to undergo capacitation,[52] and the responsiveness toward the guidance mechanisms is only observed in capacitated sperm.[53] Capacitated sperm selected by thermotaxis have been shown to improve the ART outcome in mice.[53] In this study, we showed that capacitated sperm demonstrated a stronger responsive toward DEFB119 compared with non-capacitated sperm, suggesting the potential use of DEFB119-mediated sperm chemotaxis, either used alone or in combination with another guidance mechanism, in mimicking the physiological sperm selection process in the FRT to pick the sperm in ART procedures that may improve the pregnancy outcome.

Together, our study has revealed that DEFB19/119 is a previously unsuspected physiological chemoattractant, contributing significantly to sperm chemotaxis essential for successful fertilization. Defects of DEFB19/119 may underlie idiopathic infertility.

Limitations of the study

Our results showed that knockout of *Defb19* in mice results in female subfertility, while mutations of the *DEFB119* gene are associated with idiopathic infertility. While DEFB19/119 both activate the CatSper channel, the potential difference in the physiological contributions of DEFB19/119-mediated sperm chemotaxis in the fecundity of human and mice remains to be investigated. Besides, while a number of polymorphisms/mutations were identified in idiopathic infertile women, how these heterozygous polymorphisms and mutations contribute to the lowered expression level or function of DEFB119 in the FF has not been investigated in the present study.

STAR★METHODS

Detailed methods are provided in the online version of this paper and include the following:

- KEY RESOURCES TABLE
- RESOURCE AVAILABILITY
  - Lead contact
  - Materials availability
  - Data and code availability
- EXPERIMENTAL MODEL AND SUBJECT DETAILS
  - Animals
  - Clinical samples
- METHOD DETAILS
  - Preparations of sperm
  - Animal models
  - Mouse cumulus-cell primary culture
  - Reverse transcription and real-time PCR
  - Western blot
  - Immunofluorescence staining
  - Intracellular Ca^{2+} measurement
  - Sperm ascending accumulation gradient assay (AAGA)
  - Sperm choice assay
  - Directionality-based assay
  - Sperm kinetic parameters and hyperactivity assay
  - Sperm patch-clamp recordings
  - ELISA
- QUANTIFICATION AND STATISTICAL ANALYSIS

Cell Reports Medicine
Article

CellPress
OPEN ACCESS

REFERENCES

1. Isaksson, R., and Tiitinen, A. (2004). Present concept of unexplained infertility. Gynecol. Endocrinol. *18*, 278–290.

2. Miki, K., and Clapham, D.E. (2013). Rheotaxis guides mammalian sperm. Curr. Biol. *23*, 443–452. https://doi.org/10.1016/j.cub.2013.02.007.

3. Perez-Cerezales, S., Boryshpolets, S., and Eisenbach, M. (2015). Behavioral mechanisms of mammalian sperm guidance. Asian J. Androl. *17*, 628–632. https://doi.org/10.4103/1008-682X.154308.

4. Pérez-Cerezales, S., Boryshpolets, S., Afanzar, O., Brandis, A., Nevo, R., Kiss, V., and Eisenbach, M. (2015). Involvement of opsins in mammalian sperm thermotaxis. Sci. Rep. *5*, 16146. https://doi.org/10.1038/srep16146.

5. Kantsler, V., Dunkel, J., Blayney, M., and Goldstein, R.E. (2014). Rheotaxis facilitates upstream navigation of mammalian sperm cells. Elife *3*, e02403. https://doi.org/10.7554/eLife.02403.

6. Zaferani, M., Cheong, S.H., and Abbaspourrad, A. (2018). Rheotaxis-based separation of sperm with progressive motility using a microfluidic corral system. Proc. Natl. Acad. Sci. USA *115*, 8272–8277. https://doi.org/10.1073/pnas.1800819115.

7. Zhang, Z., Liu, J., Meriano, J., Ru, C., Xie, S., Luo, J., and Sun, Y. (2016). Human sperm rheotaxis: a passive physical process. Sci. Rep. *6*, 23553. https://doi.org/10.1038/srep23553.

8. Kaupp, U.B., Kashikar, N.D., and Weyand, I. (2008). Mechanisms of sperm chemotaxis. Annu. Rev. Physiol. *70*, 93–117. https://doi.org/10.1146/annurev.physiol.70.113006.100654.

9. Eisenbach, M., and Giojalas, L.C. (2006). Sperm guidance in mammals—an unpaved road to the egg. Nat. Rev. Mol. Cell Biol. *7*, 276–285.

10. Eisenbach, M. (1999). Sperm chemotaxis. Rev. Reprod. *4*, 56–66.

11. Sun, F., Bahat, A., Gakamsky, A., Girsh, E., Katz, N., Giojalas, L.C., Tur-Kaspa, I., and Eisenbach, M. (2005). Human sperm chemotaxis: both the oocyte and its surrounding cumulus cells secrete sperm chemoattractants. Hum. Reprod. *20*, 761–767.

12. Armon, L., Ben-Ami, I., Ron-El, R., and Eisenbach, M. (2014). Human oocyte-derived sperm chemoattractant is a hydrophobic molecule associated with a carrier protein. Fertil. Steril. *102*, 885–890. https://doi.org/10.1016/j.fertnstert.2014.06.011.

13. Teves, M.E., Barbano, F., Guidobaldi, H.A., Sanchez, R., Miska, W., and Giojalas, L.C. (2006). Progesterone at the picomolar range is a chemoattractant for mammalian spermatozoa. Fertil. Steril. *86*, 745–749.

14. Strünker, T., Goodwin, N., Brenker, C., Kashikar, N.D., Weyand, I., Seifert, R., and Kaupp, U.B. (2011). The CatSper channel mediates progesterone-induced Ca 2+ influx in human sperm. Nature *471*, 382–386.

15. Lishko, P.V., Botchkina, I.L., and Kirichok, Y. (2011). Progesterone activates the principal Ca 2+ channel of human sperm. Nature *471*, 387–391.

16. Spehr, M., Gisselmann, G., Poplawski, A., Riffell, J.A., Wetzel, C.H., Zimmer, R.K., and Hatt, H. (2003). Identification of a testicular odorant receptor mediating human sperm chemotaxis. Science *299*, 2054–2058.

17. Pazgier, M., Hoover, D.M., Yang, D., Lu, W., and Lubkowski, J. (2006). Human β-defensins. Cell. Mol. Life Sci. *63*, 1294–1313.

18. Zhou, C.X., Zhang, Y.-L., Xiao, L., Zheng, M., Leung, K.M., Chan, M.Y., Lo, P.S., Tsang, L.L., Wong, H.Y., Ho, L.S., et al. (2004). An epididymis-specific β-defensin is important for the initiation of sperm maturation. Nat. Cell Biol. *6*, 458–464.

19. Tollner, T.L., Venners, S.A., Hollox, E.J., Yudin, A.I., Liu, X., Tang, G., Xing, H., Kays, R.J., Lau, T., Overstreet, J.W., et al. (2011). A common mutation in the defensin DEFB126 causes impaired sperm function and subfertility. Sci. Transl. Med. *3*, 92ra65.

20. Xu, W., Zhang, X., Chen, W., Fok, K.L., Rowlands, D.K., Chui, Y.-L., and Chan, H.C. (2010). Immunization with Bin1b decreases sperm motility with compromised fertility in rats. Fertil. Steril. *93*, 952–958.e1.

21. Diao, R., Fok, K.L., Chen, H., Yu, M.K., Duan, Y., Chung, C.M., Li, Z., Wu, H., Li, Z., Zhang, H., et al. (2014). Deficient human β-defensin 1 underlies male infertility associated with poor sperm motility and genital tract infection. Sci. Transl. Med. *6*, 249ra108.

22. Byers, S.L., Wiles, M.V., Dunn, S.L., and Taft, R.A. (2012). Mouse estrous cycle identification tool and images. PLoS One *7*, e35538.

23. Zhao, B.C., Lin, H.C., Yang, D., Ye, X., and Li, Z.G. (2015). Disulfide bridges in defensins. Curr. Top. Med. Chem. *16*, 206–219. https://doi.org/10.2174/1568026615666150701115911.

24. Wu, Z., Hoover, D.M., Yang, D., Boulègue, C., Santamaria, F., Oppenheim, J.J., Lubkowski, J., and Lu, W. (2003). Engineering disulfide bridges to dissect antimicrobial and chemotactic activities of human beta-defensin 3. Proc. Natl. Acad. Sci. USA *100*, 8880–8885. https://doi.org/10.1073/pnas.1533186100.

25. Yu, H., Dong, J., Gu, Y., Liu, H., Xin, A., Shi, H., Sun, F., Zhang, Y., Lin, D., and Diao, H. (2013). The novel human beta-defensin 114 regulates lipopolysaccharide (LPS)-mediated inflammation and protects sperm from motility loss. J. Biol. Chem. *288*, 12270–12282. https://doi.org/10.1074/jbc.M112.411884.

26. Fabro, G., Rovasio, R.A., Civalero, S., Frenkel, A., Caplan, S.R., Eisenbach, M., and Giojalas, L.C. (2002). Chemotaxis of capacitated rabbit spermatozoa to follicular fluid revealed by a novel directionality-based assay. Biol. Reprod. *67*, 1565–1571.

27. Armon, L., and Eisenbach, M. (2011). Behavioral mechanism during human sperm chemotaxis: involvement of hyperactivation. PLoS One *6*, e28359.

28. Armon, L., Caplan, S.R., Eisenbach, M., and Friedrich, B.M. (2012). Testing human sperm chemotaxis: how to detect biased motion in population assays. PLoS One *7*, e32909.

29. Ren, D., and Xia, J. (2010). Calcium signaling through CatSper channels in mammalian fertilization. Physiology *25*, 165–175.

30. Diao, R., Wang, T., Fok, K.L., Li, X., Ruan, Y., Yu, M.K., Cheng, Y., Chen, Y., Chen, H., Mou, L., et al. (2017). CCR6 is required for ligand-induced CatSper activation in human sperm. Oncotarget *8*, 91445–91458.

31. Strünker, T., Goodwin, N., Brenker, C., Kashikar, N.D., Weyand, I., Seifert, R., and Kaupp, U.B. (2011). The CatSper channel mediates progesterone-induced Ca2+ influx in human sperm. Nature *471*, 382–386. https://doi.org/10.1038/nature09769.

32. Lishko, P.V., Botchkina, I.L., and Kirichok, Y. (2011). Progesterone activates the principal Ca2+ channel of human sperm. Nature *471*, 387–391. https://doi.org/10.1038/nature09767.

33. Ren, D., Navarro, B., Perez, G., Jackson, A.C., Hsu, S., Shi, Q., Tilly, J.L., and Clapham, D.E. (2001). A sperm ion channel required for sperm motility and male fertility. Nature *413*, 603–609. https://doi.org/10.1038/35098027.

34. Xia, J., Reigada, D., Mitchell, C.H., and Ren, D. (2007). CATSPER channel-mediated Ca2+ entry into mouse sperm triggers a tail-to-head propagation. Biol. Reprod. *77*, 551–559. https://doi.org/10.1095/biolreprod.107.061358.

35. Chávez, J.C., De la Vega-Beltrán, J.L., José, O., Torres, P., Nishigaki, T., Treviño, C.L., and Darszon, A. (2018). Acrosomal alkalization triggers Ca(2+) release and acrosome reaction in mammalian spermatozoa. J. Cell. Physiol. *233*, 4735–4747. https://doi.org/10.1002/jcp.26262.

36. Singh, A.P., and Rajender, S. (2015). CatSper channel, sperm function and male fertility. Reprod. Biomed. Online *30*, 28–38.

37. Brenker, C., Goodwin, N., Weyand, I., Kashikar, N.D., Naruse, M., Krähling, M., Müller, A., Kaupp, U.B., and Strünker, T. (2012). The CatSper channel: a polymodal chemosensor in human sperm. EMBO J. *31*, 1654–1665.

38. Chang, H., and Suarez, S.S. (2010). Rethinking the relationship between hyperactivation and chemotaxis in mammalian sperm. Biol. Reprod. *83*, 507–513.

39. Ded, L., Hwang, J.Y., Miki, K., Shi, H.F., and Chung, J.J. (2020). 3D in situ imaging of female reproductive tract reveals molecular signatures of fertilizing spermatozoa in mice. Elife *9*, e62043.

40. Chung, J.J., Shim, S.H., Everley, R.A., Gygi, S.P., Zhuang, X., and Clapham, D.E. (2014). Structurally distinct Ca^{2+} signaling domains of sperm flagella orchestrate tyrosine phosphorylation and motility. Cell *157*, 808–822.

41. Guidobaldi, H.A., Teves, M.E., Uñates, D.R., and Giojalas, L.C. (2012). Sperm transport and retention at the fertilization site is orchestrated by a chemical guidance and oviduct movement. Reproduction *143*, 587–596.

42. Radhakrishnan, Y., Fares, M.A., French, F.S., Hall, S.H., and %. (2007). Comparative genomic analysis of a mammalian beta-defensin gene cluster. Physiol. Genom. *30*, 213–222.

43. Rennhack, A., Schiffer, C., Brenker, C., Fridman, D., Nitao, E.T., Cheng, Y.M., Tamburrino, L., Balbach, M., Stölting, G., Berger, T.K., et al. (2018). A novel cross-species inhibitor to study the function of CatSper Ca(2+) channels in sperm. Br. J. Pharmacol. *175*, 3144–3161. https://doi.org/10.1111/bph.14355.

44. Ottaviano, G., Zuccarello, D., Menegazzo, M., Perilli, L., Marioni, G., Frigo, A.C., Staffieri, A., and Foresta, C. (2013). Human olfactory sensitivity for bourgeonal and male infertility: a preliminary investigation. Eur. Arch. Oto-Rhino-Laryngol. *270*, 3079–3086. https://doi.org/10.1007/s00405-013-2441-0.

45. Sinding, C., Kemper, E., Spornraft-Ragaller, P., and Hummel, T. (2013). Decreased perception of bourgeonal may be linked to male idiopathic infertility. Chem. Senses *38*, 439–445. https://doi.org/10.1093/chemse/bjt009.

46. Ng, P.C., and Henikoff, S. (2001). Predicting deleterious amino acid substitutions. Genome Res. *11*, 863–874.

47. Adzhubei, I.A., Schmidt, S., Peshkin, L., Ramensky, V.E., Gerasimova, A., Bork, P., Kondrashov, A.S., and Sunyaev, S.R. (2010). A method and server for predicting damaging missense mutations. Nat. Methods *7*, 248–249.

48. Jagadeesh, K.A., Wenger, A.M., Berger, M.J., Guturu, H., Stenson, P.D., Cooper, D.N., Bernstein, J.A., and Bejerano, G. (2016). M-CAP eliminates a majority of variants of uncertain significance in clinical exomes at high sensitivity. Nat. Genet. *48*, 1581–1586. https://doi.org/10.1038/ng.3703.

49. Jagadeesh, K.A., Wenger, A.M., Berger, M.J., Guturu, H., Stenson, P.D., Cooper, D.N., Bernstein, J.A., and Bejerano, G. (2016). M-CAP eliminates a majority of variants of uncertain significance in clinical exomes at high sensitivity. Nat. Genet. *48*, 1581–1586.

50. Miller, M.R., Mannowetz, N., Iavarone, A.T., Safavi, R., Gracheva, E.O., Smith, J.F., Hill, R.Z., Bautista, D.M., Kirichok, Y., and Lishko, P.V. (2016). Unconventional endocannabinoid signaling governs sperm activation via the sex hormone progesterone. Science *352*, 555–559. https://doi.org/10.1126/science.aad6887.

51. Practice Committee of the American Society for Reproductive Medicine (2006). Effectiveness and treatment for unexplained infertility. Fertil. Steril. *86*, S111–S114. https://doi.org/10.1016/j.fertnstert.2006.07.1475.

52. Cohen-Dayag, A., Tur-Kaspa, I., Dor, J., Mashiach, S., and Eisenbach, M. (1995). Sperm capacitation in humans is transient and correlates with chemotactic responsiveness to follicular factors. Proc. Natl. Acad. Sci. USA *92*, 11039–11043. https://doi.org/10.1073/pnas.92.24.11039.

53. Pérez-Cerezales, S., Laguna-Barraza, R., de Castro, A.C., Sánchez-Calabuig, M.J., Cano-Oliva, E., de Castro-Pita, F.J., Montoro-Buils, L., Pericuesta, E., Fernández-González, R., and Gutiérrez-Adán, A. (2018). Sperm selection by thermotaxis improves ICSI outcome in mice. Sci. Rep. *8*, 2902. https://doi.org/10.1038/s41598-018-21335-8.

54. World Health Organization (2010). WHO Laboratory Manual for the Examination and Processing of Human Semen (World Health Organization).

55. Finkelstein, M., Etkovitz, N., and Breitbart, H. (2010). Role and regulation of sperm gelsolin prior to fertilization. J. Biol. Chem. *285*, 39702–39709.

56. Wang, S., and Larina, I.V. (2018). In vivo three-dimensional tracking of sperm behaviors in the mouse oviduct. Development *145*, dev.157685.

57. Caligioni, C.S. (2009). Assessing reproductive status/stages in mice. Curr. Protoc. Neurosci. *Appendix 4*. Appendix 4I.

58. Nishimura, H., Kim, E., Nakanishi, T., and Baba, T. (2004). Possible function of the ADAM1a/ADAM2 fertilin complex in the appearance of ADAM3 on the sperm surface. J. Biol. Chem. *279*, 34957–34962.

59. Kim, E., Yamashita, M., Nakanishi, T., Park, K.E., Kimura, M., Kashiwabara, S.i., and Baba, T. (2006). Mouse sperm lacking ADAM1b/ADAM2 fertilin can fuse with the egg plasma membrane and effect fertilization. J. Biol. Chem. *281*, 5634–5639.

60. Relloso, M., and Esponda, P. (2000). In-vivo transfection of the female reproductive tract epithelium. Mol. Hum. Reprod. *6*, 1099–1105.

61. Smith, T.T., and Yanagimachi, R. (1990). The viability of hamster spermatozoa stored in the isthmus of the oviduct: the importance of sperm-epithelium contact for sperm survival. Biol. Reprod. *42*, 450–457.

62. Smith, T.T., and Yanagimachi, R. (1991). Attachment and release of spermatozoa from the caudal isthmus of the hamster oviduct. J. Reprod. Fertil. *91*, 567–573.

63. Yeung, C.H., Wagenfeld, A., Nieschlag, E., and Cooper, T.G. (2000). The cause of infertility of male c-ros tyrosine kinase receptor knockout mice. Biol. Reprod. *63*, 612–618.

64. Guidobaldi, H.A., Teves, M.E., Uñates, D.R., and Giojalas, L.C. (2012). Sperm transport and retention at the fertilization site is orchestrated by a chemical guidance and oviduct movement. Reproduction *143*, 587–596.

65. Tacconis, P., Revelli, A., Massobrio, M., Battista La Sala, G., and Tesarik, J. (2001). Chemotactic responsiveness of human spermatozoa to follicular fluid is enhanced by capacitation but is impaired in dyspermic semen. J. Assist. Reprod. Genet. *18*, 36–44.

66. Schatten, H. (2004). Germ Cell Protocols (Springer Berlin), p. 254.

67. Villanueva-Díaz, C., Arias-Martínez, J., Bustos-López, H., and Vadillo-Ortega, F. (1992). Novel model for study of human sperm chemotaxis. Fertil. Steril. *58*, 392–395.

68. Stutte, S., Quast, T., Gerbitzki, N., Savinko, T., Novak, N., Reifenberger, J., Homey, B., Kolanus, W., Alenius, H., and Förster, I. (2010). Requirement of CCL17 for CCR7-and CXCR4-dependent migration of cutaneous dendritic cells. Proc. Natl. Acad. Sci. USA *107*, 8736–8741.

69. Mortimer, S.T., Swan, M.A., and Mortimer, D. (1998). Effect of seminal plasma on capacitation and hyperactivation in human spermatozoa. Hum. Reprod. *13*, 2139–2146.

70. Nassar, A., Mahony, M., Blackmore, P., Morshedi, M., Ozgur, K., and Oehninger, S. (1998). Increase of intracellular calcium is not a cause of pentoxifylline-induced hyperactivated motility or acrosome reaction in human sperm 4. Fertil. Steril. *69*, 748–754.

71. Goodson, S.G., Zhang, Z., Tsuruta, J.K., Wang, W., and O'Brien, D.A. (2011). Classification of mouse sperm motility patterns using an automated multiclass support vector machines model. Biol. Reprod. *84*, 1207–1215. https://doi.org/10.1095/biolreprod.110.088989.

72. Olds-Clarke, P., and Sego, R. (1992). Calcium alters capacitation and progressive motility of uterine spermatozoa from +/+ and congenic tw32/+ mice. Biol. Reprod. *47*, 629–635.

73. Mortimer, S.T. (2000). CASA–practical aspects. J. Androl. *21*, 515–524.

STAR★METHODS

KEY RESOURCES TABLE

REAGENT or RESOURCE	SOURCE	IDENTIFIER
Antibodies		
Normal Rabbit IgG	Santa Cruz	Cat# sc-2027; RRID:AB_7371977
Normal Goat IgG	Santa Cruz	Cat# sc-2028;RRID:AB_737167
Normal Mouse IgG	Santa Cruz	Cat# sc-2025;RRID:AB_737182
anti-Catsper1 (H300)	Santa Cruz	Cat# sc-33153;RRID:AB_2259786
anti-Catsper1 (D-17)	Santa Cruz	Cat# sc-21180;RRID:AB_2071879
anti-Catsper1 (N-term)	Abgent Biotechnology	Cat# AP12995a;RRID:AB_10820829
Anti-Catsper1 (extracellular)	Thermo Fisher Scientific	Cat# PA5-77359;RRID:AB_2735579
Goat polyclonal antibodies to DEFB19	Abcam	Cat# ab126867;RRID:AB_11130326
Rabbit polyclonal antibodies to DEFB119	Abcam	Cat# ab122826;RRID:AB_11128981
Biological samples		
Human semen	Peking University Shenzhen Hospital	N/A
Human follicular fluid	Jiangsu Province Hospital.	N/A
Human peripheral blood	Jiangsu Province Hospital.	N/A
Chemicals, peptides, and recombinant proteins		
Lipofectamine 3000	Invitrogen	Cat# L3000-015
Recombinant mouse active DEFB19	This paper	N/A
GST-DEFB119	Cloud-Clone Corp	Cat# RPQ653Hu01
GST tag	Abcam	Cat# ab70456
Percoll	SAGE Media	Cat# 2080; Cat# 2040
HEPES	Gibco	Cat# 15630080
Sodium Lactate	Sigma-Aldrich	Cat# 71718
Hoechst 33258	Thermo Fisher	Cat# H1398
Penicillin-Streptomycin	Gibco	Cat# 15140122
DMEM/F12	Gibco	Cat# 11330-032
Critical commercial assays		
mMESSAGE mMACHINE™ T7 ULTRA	Ambion	Cat# AM1345
MEGAshortscript Kit	Thermo Fisher Scientific	Cat# AM1354
TRIzol Reagent	Thermo Fisher Scientific	Cat# 15596026
High Capacity cDNA Reverse Transcription Kits	Applied Biosystems	Cat# 4368814
SYBGreen master mix	Takara	Cat# RR42LR
Pierce ECL Western Blotting Substrate	Thermo Fisher Scientific	Cat# 32209
Pierce BCA Protein Assay Kit Cat#23225	Thermo Fisher Scientific	Cat# 23225
ProLong Gold Antifade Mountant with DAPI	Invitrogen	Cat# P36935
Transwell	Merk	Cat# 38024
μ-Slide Chemotaxis[3D]	ibidi	Cat# 80326
DEFB19 ELISA Kit	Cloud-Clone Corp	Cat# SEQ653Mu
DEFB119 ELISA Kit	LifeSpan BioSciences	Cat# LS-F13148
Experimental models: Organisms/strains		
Defb19-KO mouse model	This paper	N/A
CatSper1-KO mouse model	This paper	N/A
Oligonucleotides		
Primers for q-PCR or Clone	Table S3	N/A

(Continued on next page)

Continued

REAGENT or RESOURCE	SOURCE	IDENTIFIER
siDefb19	Thermo Fisher Scientific	Cat# 1320001
Software and algorithms		
ImageJ	National Institutes of Health	https://imagej.nih.gov/ij/index.html
Manual Tracking	Fabrice Cordelires, Institut Curie, Orsay (France).	https://imagej.nih.gov/ij/plugins/track/track.html
Chemotaxis and Migration Tool	R Zantl, E Horn	https://ibidi.com/chemotaxis-analysis/171-chemotaxis-and-migration-tool.html

RESOURCE AVAILABILITY

Lead contact
Further information and request for resources and reagents should be directed to and will be fulfilled by the lead contact, Dr. Kin Lam Fok (ellisfok@cuhk.edu.hk).

Materials availability
This study did not generate new unique reagents.

Data and code availability
All data reported in this paper will be shared by the lead contact upon request. This paper does not report the original code. Any additional information required to reanalyze the data reported in this paper is available from the lead contact upon request.

EXPERIMENTAL MODEL AND SUBJECT DETAILS

Animals
ICR mice were purchased from the Laboratory Animal Service Center of the Chinese University of Hong Kong. All experiments were conducted in accordance with the University Laboratory Animals Service Center's guidelines on animal experimentation with approval from the Animal Ethics Committee of the University (Reference number: 14-043-GRF) and Laboratory Animal Center of Nantong University (Reference number: S20200312-018).

Clinical samples
Procedures for human sperm collection were approved by the Regional Committee for Medical Research Ethics and the Human Ethics Committee of Peking University Shenzhen Hospital. Written consents were obtained from each subject. Normal human semen was obtained from 20- to 42-year-old healthy donors categorized according to World Health Organization Criteria,[54] with the details provided below: a sperm concentration of $\geq 20 \times 10^6$ spermatozoa/mL, sperm motility with forward progression $\geq 32\%$, and normal morphology $\geq 4\%$.

Procedures for the follicular fluid collection were approved by The Joint Chinese University of Hong Kong-New Territories East Cluster Clinical Research Ethics Committee and Ethics Committee of Jiangsu Province Hospital. Written consents were obtained from each subject. Unexplained infertility follicular fluid collection was approved by the Peking University Shenzhen Hospital Ethics Committee (PKUSZH [2019]008).

METHOD DETAILS

Preparations of sperm
Mouse sperm was obtained from cauda epididymis of 10-weeks old ICR mice. Briefly, excised cauda epididymis was rinsed and cut in 1 mL of sperm washing medium (SWM) comprising: 97.8 mM NaCl, 4.69 mM KCl, 2.04 mM $CaCl_2.2H_2O$, 0.2 mM $MgSO_4.7H_2O$, 4 mM $NaHCO_3$, 21 mM HEPES (pH 7.4), 21.4 mM sodium lactate, 2.78 mM Glucose, 5 mg/L Phenol Red, 5 mg/mL BSA. Immediately following dispersion of sperm into the medium, the sperm-containing suspension was transferred to a 15 mL plastic tube. For *in vitro* capacitation, the sperm was incubated at 37°C with 5% CO_2 in SWM for 2 h.

Human semen was collected by masturbation after 3- to 5-day sexual abstinence. After complete liquefaction at 37°C for 30 min, sperm was purified from liquefied semen by Percoll centrifugation before assays. Parameters including semen volume, sperm motility, sperm viability, and sperm concentration were analyzed by a computer-assisted semen analysis (CASA) system under 100× magnifications. Human sperm was capacitated in capacitation medium (Ham's F-10) supplemented with 3 mg/mL BSA for 3 h at 37°C in 5% CO_2.[55]

Animal models

Adult females were monitored for estrous cycle through an established protocol.[56,57]

In the oviduct ligation model, at the estrous phase, female mice at 10 weeks of age were anaesthetized with Ketamine (75 mg/kg, ip) and Xylazine (10 mg/kg, ip). Two incisions were made at the back of the mice to expose both sides of the ovary and the oviduct. Oviduct was surgically tied at the fimbriae level in the experimental group, leaving the contralateral oviduct untied as a sham control. After recovery for 48 h, female mice were housed with male mice for mating. Mating was confirmed by the presence of a vaginal plug which was observed every 30 min as described previously[58,59] and female mice were sacrificed at 6–8 h post-coitus for sperm and tissues collection.[39,40]

For overexpression of DEFB19 in oviduct ligation model, the oviducts were injected with 20 μL DNA/liposome complexes (Lipofectamine 3000) containing 2 μg of DNA (pcDNA3.1-Defb19) using a thin injection capillary via fimbriae as described previously.[60] After injection, both sides of oviduct were ligated as described above. Western-blot or immunofluorescence were used to confirm the efficiency of oviduct transfection. After recovery for 48 h, female mice were housed with male mice for mating. Mating was confirmed by the presence of a vaginal plug which was observed every 30 min and female mice were sacrificed at 6–8 h post-coitus for sperm and tissues collection.

For knockdown of DEFB19, at the estrous phase, female mice oviducts were exposed as described above. 20 μL siRNA/liposome complexes containing 50 pmol siRNA (siDefb19) were injected into the oviducts. Western-blot or immunofluorescence were performed to examine the efficiency of oviduct transfection. After recovery for 48 h, female mice were mated with male mice. Mating was confirmed by the presence of a vaginal plug which was observed every 30 min and female mice were sacrificed at 6–8 h post-coitus for sperm and tissues collection. Mated female mice were housed for another 7 days for evaluating the number of implanted embryos.

For analysis of oviductal sperm, sperm were obtained by the three-step flushing protocol as described previously.[61–63] Briefly, oviducts were carefully separated from the uterine horns and straightened out by cutting the mesosalpinx. Oviducts were gently washed with sperm washing medium (SWM) to remove sperm attached to the outside wall. The first loop of the ampulla was ligated (for no ligated model) and pierced with a micropipette attached to a glass syringe mounted in a microinjector. Each oviduct was flushed first with 20 μL SWM and then left for 3–4 min before being flushed with another 20 μL SWM. Each oviduct was then flushed a third time with 40 μL SWM containing Triton X-100 (0.2%, v/v) to remove spermatozoa that had firmly attached to the mucosal surface. The flushes were centrifuged at 5000 g for 10 min; the pellet was resuspended in a solution of 5% formaldehyde and 0.1 mg/mL Hoechst 33258 in PBS, for 15 min at room temperature. The samples were washed twice with distilled water at 5000 g for 10 min. The pellet was resuspended in distilled water, spreading it on a slide. The total number of spermatozoa recovered from the oviduct lumen was counted under simultaneous phase contrast and fluorescent illumination at 400× as described previously.[64]

Defb19-KO mouse model was generated by Cyagen Biosciences Inc. The guide RNAs were designed targeting exon 1 and exon 2 of *Defb19*. Cas9 mRNA and gRNA generated by *in vitro* transcription were then injected into fertilized eggs for KO mouse productions. The injected embryos were transferred into the oviducts of pseudopregnant mice. All the mice were maintained in a C57BL/6 background. *Defb19* heterozygote male mice were mated with *Defb19* heterozygote female mice to produce *Defb19*-KO offspring. DNA isolated from tail biopsies was used for genotyping. The founders were genotyped by PCR followed by DNA sequencing analysis. The primers for PCR and real-time PCR are listed in Table S3.

CatSper1-KO mouse model was generated by Shanghai Model Organisms Center, Inc (Shanghai, China). The guide RNAs were designed targeting intron 1 and intron 4 of Catsper 1 gene to generate the deleted exon 2–4 mutant mouse. Briefly, Cas9 mRNA was transcribed with mMESSAGE mMACHINE T7 Ultra Kit (Ambion, TX, USA) according to the manufacturer's instructions. Two sgRNAs targeted to delete exons 2–4 were *in vitro* transcribed using the MEGAshortscript Kit (ThermoFisher, USA). One sgRNA targeted to intron 1of gene *Catsper1* was 5'- GCTTGTCCTGTTCTGGCCTT -3'; the other sgRNA targeted to intron 4 of gene *Catsper1* was 5'- GGGGTTCCGTGGGACATGTT -3'. *In vitro*-transcribed Cas9 mRNA and sgRNAs were injected into zygotes of C57BL/6J mouse, and transferred to pseudopregnant recipients. Obtained F0 mice were validated by PCR and sequencing using primer pairs: F- 5'-CAAACTGGGCCCCTGATGTGGA-3'; R-5'-GTGGGCAGTGATGGAGAGGGAGTC-3'. The positive F0 mice were chosen and crossed with C57BL/6J mice to obtain F1 heterozygous *Catsper1* knockout mice. The genotype of F1 mice was identified by PCR and confirmed by sequencing. Male and female F1 heterozygous mice were intercrossed to produce the homozygous *Catsper1* knockout mice.

For artificial insemination, female mice (10 weeks old) were hormonally stimulated with 5 IU of pregnant mare serum gonadotrophin (PMSG), and 2 IU hCG was injected intraperitoneally 48 h later. Artificial insemination was conducted by depositing 50 μL containing 3–5×10⁶ capacitated spermatozoa of WT male mice into the *Defb19*-KO female uterus via the cervix. Subsequently, the female mice were mated with sterile, vasoligated male immediately to develop a vaginal plug. Artificial inseminated female mice were sacrificed at 12–16 h post-coitus for sperm and tissues collection. Female mice were housed for another 7 days for evaluating the number of implanted embryos.

Mouse cumulus-cell primary culture

Female mice with bodyweight 18–20 g obtained from CUHK animal house. After intraperitoneal injection of PMSG 10U for 36–48 h, mice were euthanized and ovaries were excised and washed in sterilized PBS. The ovaries were incubated at 37°C and 5% CO$_2$ for

15 min in DMEM/F12 medium. The cumulus cells were released to the medium by puncture with 1 mL syringe. The cumulus cells were dispersed by 1 g/L hyaluronidase for 2 min and seeded in the culture medium (DMEM/F12+100 IU penicillin+100 IU streptomycin+10% FBS). Erythrocytes were removed by changing the medium the next day.

Reverse transcription and real-time PCR

Total RNA was extracted using TRIzol Reagent according to the manufacturer's instruction. RNA concentration level was measured by NanoVue UV/Vis Spectrophotometer (GE healthcare). 1–4 μg total RNA was used for reverse transcription using High-Capacity cDNA Reverse Transcription Kits (Applied Biosystems). Real-time PCR was carried out in Applied Biosystems QS7 384-well Real-Time PCR System using SYBGreen master mix (Takara). The sequence of primers used in this study was listed in Table S3. Gene expression was analyzed by using $2^{-\triangle\triangle_{CT}}$ method.

Western blot

A total of 2×10^8 spermatozoa were collected from the caudal epididymis of adult male mice and washed in PBS by centrifuging at 3000 rpm for 5 min. Sperm was lyzed by RIPA buffer on ice for 30 min and then in the ultrasound using the following cycle: 40 power, ultrasonic 4 s and stop 10 s and repeat 20 times. The lysates were centrifuged at 14000 rpm for 30 min. 60 μg total protein was mixed with 4× sample loading buffer and loaded into 15% sodium dodecyl sulfate-polyacrylamide gel for electrophoresis. Separated protein was transferred to 0.22 μm pore-size PVDF membrane. The PVDF membrane was blocked with 5% nonfat milk in Tris-buffered saline and immunoblotted with indicated primary antibodies diluted in 1% milk at 4°C overnight. On the next day, the membrane was washed three times with TBST for 10 min each, and then incubated with 1:10000 diluted horseradish peroxidase-linked secondary antibody in the 1% milk for 2 h at RT. The membrane was washed three times with TBST for 10 min each. Signals were detected with ECL reagent (Amersham) on Super X-film (Fuji Medical).

Immunofluorescence staining

Tissues were fixed in 4% paraformaldehyde and embedded in OCT. Five-micrometer sections were prepared from embedded tissue. The sections were rinsed with PBS for 15 min, and the antigens were retrieved with EDTA alkaline buffer (10 mM Tris buffer, 1 mM EDTA, adjust pH to 9.0 using 1M NaOH). After 30 min cooling at the room temperature, the slides were washed in PBS three times for 5 min each. The sections were then blocked with 1% BSA in PBS for 15 min, and then incubated with primary antibodies in 1% BSA in PBS overnight at 4°C.

For immunofluorescence staining of sperm, sperm were pretreated with rDEFB19 (400 ng/mL)/GST-DEFB119 (800 ng/mL) for 30 min and collected sperm was fixed in 4% paraformaldehyde and spread onto glass slides. The samples were permeabilized in 0.5% Triton X-100 for 15 min followed by blocking with 10% normal donkey serum for 60 min. Afterward, the samples were incubated with primary antibodies overnight at 4°C.

On the next day, the slides were washed three times in PBS or PBST for 3 min each and then incubated with appropriate fluorescent-conjugated secondary antibodies at 1:500 (Molecular Probes) in PBS for 60 min at room temperature. The slides were washed three times in PBS for 3 min each and mounted with Prolong®Gold Antifade Reagent (with DAPI) (Invitrogen). Fluorescent images were captured by a fluorescent microscope (NIKON ECLIPSE 80i) or confocal microscope (OLYMPUS FV1000).

Intracellular Ca^{2+} measurement

Collected sperm was loaded with 5 μM fluo-4AM, 1.5 μM Pluronic F-127 in modified sperm washing medium in the dark at 35°C for 30 min. After loading, sperm was washed once with fresh sperm washing medium. To start the experiment, sperm suspensions were added on a coverslip precoated with 10% Poly-L-lysine (0.01% w/v) for 2 min. Unattached sperm was removed by gently washing, and the chamber was filled with sperm washing medium. Treatments were added to the medium at the indicated time point as shown in the time-trace curve. Measurements were made on an Eclipse fluorescence microscope (Nikon Eclipse Ti) with a 60× oil objective lens (1.40 NA) (Nikon) and a CCD camera (Spot Xplorer) controlled by the software MetaFluor (Universal Imaging). Excitation at 488 nm was used and emission was collected at 510 nm.

Sperm ascending accumulation gradient assay (AAGA)

Chemotaxis chambers (24-well format) with 8.0-μm pore size, tissue culture-treated polycarbonate membrane filter, 10 μm thick, having a total area of 6.5 mm^2 (Transwell; Costar, Cambridge, MA, USA), were used as previously reported.[65,66] In brief, 600 μL of capacitated sperm suspension at a density of 1–2×10^6 cell/mL was added to the lower compartment. The upper wells were separated from the lower ones by a polycarbonate Nucleopore filter (8-μm pore diameter) and a gasket. To induce chemotaxis, indicated amount of recombinant DEFB19/119 or vehicle control was added to the upper wells. The chamber was incubated at 37°C with 5% CO$_2$ for 30 min. Then, 10 μL of the medium was collected from the upper compartment and the number of sperm was immediately counted by a hemacytometer.

Sperm choice assay

We customized a double-chamber model as shown in Figure S2 using plexiglass, which is similar to the device described previously.[67] Before the experiment, the chamber was anchored on a 10 cm Petri dish, pre-incubated at 37°C for 30 min and equilibrated

with 500 μL sperm washing medium. To start the experiment, 5 μL of capacitated mouse sperm (20×10^7 cells/mL) or capacitated human sperm (30×10^7 cells/mL) were applied through the central hole. Medium to be tested and vehicle control was simultaneously added to either side of the two chambers respectively. The chamber was incubated at 37°C for 30 min and the experiments were stopped by placing two modified pipette tips in the entrance of the chambers. The solution in each chamber was transferred separately and centrifuged at 1500 g for 10 min at room temperature. Cell pellets were resuspended in sperm washing medium and a 10 μL aliquot was counted on a hemacytometer.

Directionality-based assay
The experiments were carried out at 37°C with a Zigmond-like chemotaxis chamber (μ-Slide Chemotaxis[3D]; ibidi Cat. No. 80326) as described previously[26–28] with some modifications. The chamber was pre-incubated at 37°C for 30 min. Both reservoirs and the slit were filled with capacitated sperm at a density of 4×10^6 cells/mL, the chemoattractant was applied within a sperm suspension to one of the reservoirs as indicated. The slides were incubated at 37°C for 20 min to allow the establishment of a chemoattractant concentration gradient as described previously.[27] The movement of sperm was recorded at a speed of 1 image every 0.016 s (nonstop running) for 3 s. Movement tracks of randomly selected sperm were drawn by ImageJ software with manual tracking plug-in using the frame-to-frame playback. The data was input into the chemotaxis and migration tool, which statistically analyze the direction of motion cells, to generate the tracked path and to quantify the distance as previously reported.[68] FMI (forward migration index) represent the efficiency of the forward migration of cells, and how they relate to the direction of x axes.

Sperm kinetic parameters and hyperactivity assay
Sperm kinetic parameters or hyperactivity were determined by computer-assisted semen analysis (CASA) (HTM-IVOS system, Hamilton-Thorn Research). 6 frames were acquired at a frame rate of 60 Hz. At least total 200 tracks were measured for each specimen at 37°C. We recorded at least 30 points for each tract. The playback function of the system was used to check its accuracy. Average values for sperm kinetic parameters including curvilinear velocity (VCL), straight-line velocity (VSL), average path velocity (VAP), the amplitude of lateral head displacement (ALH), linearity (LIN = VSL/VCL), and straightness (STR = VSL/VAP) were recorded. The proportion of hyperactivated spermatozoa in each sample was determined using the SORT function of the CASA instrument. In mouse sperm, hyperactivated was defined by curvilinear velocity (VCL) > 279 μm/s and an amplitude of lateral head (ALH) > 7 μm.[69–72] In human sperm, hyperactivation was defined by curvilinear velocity (VCL), >150 μm/s; linearity (LIN), <50%; half lateral head displacement ($ALH_{1/2}$), >3.5 μm.[73]

For recombinant DEFB19/119 treatment, capacitated sperm was washed with PBS and incubated with vehicle control, 400 ng/mL rDEFB19 or 800 ng/mL rDEFB119 at 37°C for 1 h followed by sperm kinetic parameters or hyperactivity analysis. In combined treatment, capacitated sperm was pre-treated with 20 μg/mL of anti-DEFB19 or anti-DEFB119 Ab or control IgG at 37°C for 1 h. Pre-treated sperm was then treated with 400 ng/mL rDEFB19 or 800 ng/mL rDEFB119 at 37°C for 1 h followed by sperm kinetic parameters or hyperactivity analysis.

Sperm patch-clamp recordings
Mouse sperm derived from *Catsper1*-KO mice were collected from male mice aged 3 months. The corpus epididymis was isolated and rinsed in high saline solution (HS: 135 mM NaCl, 5 mM KCl, 2 mM $CaCl_2$, 1 mM $MgSO_4$, 20 mM HEPES, 5 mM glucose, 10 mM lactic acid and 1 mM sodium pyruvate, pH7.4). Mouse sperm were shaken from the snipped epididymis and utilized for patch clamp. The human sperms were gently centrifuged and resuspended into HS solution to remove the seminal fluid. The patch-clamping recordings of monovalent CatSper currents in human and mouse sperm were conducted as previously described.[32] The pipettes (15–30 MΩ) for the recordings of CatSper currents containing: 135 mM cesium methanesulphonate, 5 mM CsCl, 10 mM HEPES, 10 mM EGTA (pH 7.2 with CsOH). Gigaohm seals were formed at the cytoplasmic droplet of sperm. A zap protocol (0.5 ms 450 mV–650 mV or 5 ms 350 mV–500 mV voltage application for human sperm or mouse sperm, respectively) and simultaneous light suction were performed to achieve the transition into the whole-cell configuration. The sodium-based divalent-free (Na^+ DVF) solution (150 mM sodium gluconate, 20 mM HEPES and 5 mM Na_3HEDTA; pH 7.4) was used to record the basal CatSper monovalent currents. The currents were stimulated by 1 s voltage ramp from −100 to +100 mV from a holding potential of 0 mV. Solution were applied *via* a local perfusion system allowing switching different test solution. All of the currents were recorded after >30 s perfusion of the solution. Data were analyzed with Clampfit 10.4 and GraphPad Prism 8.0. All error bars correspond to ±SD.

ELISA
The level of DEFB19/119 in follicular fluid and cumulus cell-conditioned medium were assessed by ELISA Kit for DEFB19 (Cloud-Clone Corp Cat. No. SEQ653Mu) and DEFB119 (LifeSpan BioSciences, Inc. Cat. No. LS-F13148) according to manufacturer protocol.

QUANTIFICATION AND STATISTICAL ANALYSIS

Data were expressed as mean ± SD. Differences in measured variables between two groups were calculated by Student's t-tests, and differences between more than two groups were analyzed by One-Way or Two-Way ANOVA analysis. Results were considered statistically significant at $p < 0.05$.